Title	Influence of binders and solvents on stability of Ru/RuOx nanoparticles on ITO nanocrystals as Li–O2 battery cathodes
Authors	Vankova, Svetoslava;Francia, Carlotta;Amici, Julia;Zeng, Juqin;Bodoardo, Silvia;Penazzi, Nerino;Collins, Gillian;Geaney, Hugh;O'Dwyer, Colm
Publication date	2017-01-23
Original Citation	Vankova, S., Francia, C., Amici, J., Zeng, J., Bodoardo, S., Penazzi, N., Collins, G., Geaney, H. and O'Dwyer, C. (2017) 'Influence of Binders and Solvents on Stability of Ru/RuOx Nanoparticles on ITO Nanocrystals as Li–O2 Battery Cathodes', ChemSusChem, 10(3), pp. 575-586. doi:10.1002/cssc.201601301
Type of publication	Article (peer-reviewed)
Link to publisher's version	10.1002/cssc.201601301
Rights	© 2017 Wiley-VCH Verlag GmbH &Co. KGaA, Weinheim. This is the peer reviewed version of the following article: ChemSusChem 2017, 10, 575, which has been published in final form at http://dx.doi.org/10.1002/cssc.201601301. This article may be used for non-commercial purposes in accordance with Wiley Terms and Conditions for Self-Archiving.
Download date	2023-05-05 13:46:52
Item downloaded from	http://hdl.handle.net/10468/3650

CHEMISTRY & SUSTAINABILITY

CHEMSUSCHEM

ENERGY & MATERIALS

Accepted Article

Title: The Influence of Binders and Solvents on the Stability of Ru/RuOx OER Catalyst Nanoparticles on ITO Nanocrystals in Cycled Li-O2 Battery Cathodes

Authors: Svetoslava Vankova, Carlotta Francia, Julia Amici, Juqin Zeng, Silvia Bodoardo, Nerino Penazzi, Gillian Collins, Hugh Geaney, and Colm O'Dwyer

To be cited as: *ChemSusChem* 10.1002/cssc.201601301

Link to VoR: http://dx.doi.org/10.1002/cssc.201601301

A Journal of

ChemPubSoc Europe

WILEY-VCH

www.chemsuschem.org

WILEY-VCH

FULL PAPER

The Influence of Binders and Solvents on the Stability of Ru/RuO_x OER Catalyst Nanoparticles on ITO Nanocrystals in Cycled $Li\text{-}O_2$ Battery Cathodes

Svetoslava Vankova[a], Carlotta Francia[a], Julia Amici[a], Juqin Zeng[a], Silvia Bodoardo[a], Nerino Penazzi[a], Gillian Collins[b], Hugh Geaney[b], and Colm O'Dwyer[b],[c]*

Abstract: $Li\text{-}O_2$ battery research at a fundamental level remains critical, and nature of reactions and stability are paramount for realising the promise of the $Li\text{-}O_2$ system. We report that ITO nanocrystals with supported 1-2 nm OER catalyst Ru/RuO_x nanoparticles demonstrate efficient OER processes, significantly reducing the cell's recharge overpotential, and maintain catalytic activity to promote a consistent cycling discharge potential in $Li\text{-}O_2$ cells even when the ITO support nanocrystals deteriorate from the very first cycle. The Ru/RuO_x nanoparticles lower the charge overpotential compared to ITO and carbon-only cathodes and have the greatest effect in DMSO electrolytes with a solution-processable F-free CMC binder (< 3.5 V) vs PVDF. Ru/RuO_x/ITO nanocrystalline materials in DMSO provide efficient Li_2O_2 decomposition from within the cathode during cycling. We demonstrate that the ITO is actually unstable from the first cycle and completely dissolves by chemical etching, but Ru/RuO_x NPs remain effective OER catalysts for Li_2O_2 during cycling. CMC binders avoid PVDF-based side reactions in either electrolyte, improving efficient cyclability. ITO nanocrystal deterioration is significantly mitigated in cathodes using a CMC binder, and cells show good cycle life. In mixed DMSO-EMITFSI ionic-liquid electrolytes, Ru/RuO_x/ITO materials in $Li\text{-}O_2$ cells cycle very well and maintain a consistently very low charge overpotential of 0.5 – 0.8 V.

Introduction

The recent leap of interest in the $Li\text{-}O_2$ battery reflects the need for energy-storage devices with higher energy densities than before.[1, 2, 3, 4, 5] Developing post Li-ion systems such as Li-S batteries, and advanced Li/NMC or Li/NCA Li-ion systems and a few high voltage and high capacity cathode materials, are currently some of the best alternatives available in advanced high energy density battery technology.[6] For the $Li\text{-}O_2$ system, high charge over-potentials and limited cyclability are still critical challenges to overcome. The search for highly stable electrolytes paired with stable and efficient oxygen cathodes is paramount for improving the electrochemical efficiency and performance of non-aqueous $Li\text{-}O_2$ cells[7, 8], as many recent studies on the surface composition at the electrode/electrolyte interface have underlined.[9]

As far as the oxygen electrode is concerned, there is still some debate on the real need of an electro-catalyst at the cathode of the $Li\text{-}O_2$ system,[10] yet the high oxidation potential affects efficiency and rechargeability on the cathode side. Some carbon structures, such as hierarchically porous graphene, have proven to be effective in providing large tunnels for O_2 diffusion and small pores for an ideal oxygen reduction process. Nonetheless, metals[11, 12, 13] metal alloys[14] and transition metal oxides[15, 16, 17, 18] have been investigated to catalyse both the oxygen reduction (ORR) and oxygen evolution (OER) reactions as part of the search for bi-functional catalytic reduction and oxidation of Li_2O_2.[19] In particular, Ru/RuO_x nanoparticles and nanocrystals have been shown to be effective in catalysing both processes.[20, 21] Faster OER kinetics were observed with $RuO_2{\cdot}0.64H_2O$-rGO compared to rGO itself in TEGDME-$LiCF_3SO_3$ electrolyte.[22] These electro-catalysts were, for the most part, supported on a range of structured carbons. This is because carbon is a lightweight material with good electronic conductivity and in some polymorphs has a suitable porous structure, which acts favourably for both oxygen diffusion and Li_2O_2 deposition during discharge[23]. Recent studies emphasized the instability of carbon-based cathodes in $Li\text{-}O_2$ cells, suggesting a strong dependence on the hydrophobic/hydrophilic nature of the carbon surface and its ability to promote electrolyte decomposition during cell cycling,[24] or minimize parasitic side reactions.

The net effect of the carbon-induced problems is a rapid passivation of the porous cathode and a capacity fading on cycling, primarily due to Li_2CO_3 formation, and from electrical passivation from uniformly deposited insulating Li_2O_2 that prevents charge transfer for electrochemical reactions.[25] A variety of "carbon free" cathodes has been proposed to address such issue. These have been based on nanoporous Au,[26] TiC,[27] Ru/ITO,[28] Ru/Sb-doped tin oxide,[29] nanoneedle arrays decorated with nanoflakes of transition metal oxides,[30] RuO_2/mesoporous TiO_2, [31] Ru/TiS_2 nanonets,[32] RuO_x/titanium nitride nanotube arrays,[33] and metallic mesoporous pyrochlores.[34] Of great significance is the sensitivity of the electrochemical response of the $Li\text{-}O_2$ cell to the electrolyte

[a] Dr S. Vankova, Dr C. Francia, Dr J. Amici, Dr J. Zeng, Prof. S. Bodoardo, Prof. N. Penazzi
Department of Applied Science and Technology (DISAT), Politecnico di Torino, C.so Duca degli Abruzzi 24, 10129 Torino, Italy

[b] Dr G. Collins, Dr H. Geaney, Dr C. O'Dwyer
Department of Chemistry, University College Cork, Cork, T12 YN60, Ireland

[c] Dr C. O'Dwyer
Micro-Nano Systems Centre, Tyndall National Institute, Lee Maltings, Cork, T12 R5CP, Ireland

Supporting information for this article is given via a link at the end of the document.

composition. All polar aprotic solvents used in the electrolyte react with species generated from oxygen reduction, and the extent of this reactivity with binders and the influence on cathode material stability and OER catalyst effectiveness still has some open questions. Redox mediator-based electrolytes show promise in reducing oxidation overpotential and may improve cycle life.

Ethereal solvents have been shown to enable reversible formation of lithium peroxide, although oxygen radical attack on such solvents led to their consumption during cycling.[35] DMSO allowed prolonged cell cycling when paired with carbon-free cathodes[26] but side products, mainly LiOH, were detected in some experiments when coupled with carbon-based cathodes.[36] The debate surrounding DMSO also include comprehensive experimental and theoretical investigations showing very good stability of DMSO on the Li_2O_2 surface in the presence of platinum@carbon nanotube core–shell cathodes.[37] Recently however, researchers have shown remarkable reduction in charging overpotential by stably and reversibly forming LiOH phase preferentially, or by the use of redox mediators in the electrolytes [38], pointing to alternative battery chemistries based on reversible, thermodynamically and electrochemically stable LiOH and LiO_2 phases instead of Li_2O_2.[39] Only very recently has the crystalline, stable form of the superoxide LiO_2 phase been proposed as beneficial for long cycle life Li-O_2 batteries[40].

Due to a high donor number, DMSO can stabilise the Li-superoxide intermediates. This effect abates the formation of large Li_2O_2 particles at the expense of a compact Li_2O_2 layer. The net consequence is that higher capacities can be achieved with less cathode clogging.[41] Considering electrolytes with such different characteristics, various behaviours can arise at electrolyte-cathode interface. According to Calvo *et al.*, no appreciable decomposition of DMSO occurs in the presence of insoluble Li_2O_2 until 4.2 V on the gold electrode but DMSO undergoes decomposition on Pt starting at 3.5 V.[42] The extent of parasitic reactions can be significant and depending on the type of catalyst and the electrolyte used, and on the type of polymer added to bind the material to the current collector. The net effect not only leads to a depletion of the electrolyte but also modifies the nature of the discharge products and their subsequent recharge.[43] As a result, judging electro-catalysis based solely on the over-potential reduction and on the increase of the discharge capacity, compared to a "reference" sample, is overly simplistic.[44]

In this work, we evaluate the electrochemical performance of Li-O_2 cells composed of conductive indium tin oxide (ITO) nanocrystal-supported Ru/RuO_x nanoparticles as both the electro-catalyst and discharge product host for the oxygen cathode. Ru/RuO_x/ITO was selected in order to determine the effect of side reactions at the cathode/electrolyte/binder interface derived compared to a carbon-only based cathode[28] and to investigated the stability of conductive nanocrystalline ITO support with surface-immobilized 1-2 nm Ru/RuO_x OER nanoparticles. The work also shows how changes to the cathode material affect cyclability in DMSO and TEGDME electrolytes, using PVDF or CMC binders. Electrochemical tests carried out in both $LiClO_4$-TEGDME and $LiClO_4$-DMSO solutions with a comparison examination of a mixed DMSO-ionic liquid electrolytes demonstrated how a synergistic electrolyte-catalyst choice improves long term stability and significantly reduced charge overpotential, while retaining nearly 100% efficiency and reduced energy loss (oxidation overpotential reduction). We further show that Sodium carboxymethyl cellulose (CMC) binders markedly improve long term cycling, and TEGDME-based Li-O_2 cell cycle life increased two-fold compared to identical cells using PVDF. The investigation confirms the importance of cell components stability in determining the cycling performance of the Li-O_2 cell for a given cathode material that includes a catalyst, and cathode formulations that include binders. For cathodes including effective OER catalyst such Ru/RuO_x supported on ITO, the electrolyte *and* OER catalyst (in)stability is shown not to be critical to reduce oxidation overpotential, overall cell energy efficiency and cyclability, as the Ru/RuO_x remains catalytically active towards Li_2O_2.

Results and Discussion

To develop the cathode material, ITO nanocrystalline powder was decorated with Ru/RuO_x nanoparticles. To maximize electrolyte exposure to both the ITO and Ru/RuO_x surfaces, immobilization was conducted to ensure a high degree of coverage where the Ru/RuO_x nanoparticle size is an order of magnitude less than the ITO nanocrystal size. This ensures an OER cathode and catalyst system without segregated quantities of either material; Ru/RuO_x is only located at the ITO surface. XRD patterns of the as prepared Ru/RuO_x/ITO composite is shown in Figure 1 (a). The Brunner-Emmett-Teller (BET) surface area of the final material was determined to be 25.6 $m^2 g^{-1}$.

HRTEM analysis confirmed octahedral crystalline ITO nanocrystals with dimensions in 10-50 nm range. The ITO surface-bound 1-2 nm Ru/RuO_x nanoparticles are observable in Figs 1 (b,c) (see arrows) and decorate the ITO surface without aggregation. The Ru/RuO_x NPs by this synthesis protocol do not aggregate and are immobilized on the ITO nanocrystal surface (see Supporting Information, Fig. S1).

XPS analysis was used to determine the chemical nature of the Ru/RuO_x nanoparticle surface and the binding condition to the ITO. The Ru 3d core level shown in Fig. 2 (a) is overlapped with the C 1s core level at 285 eV, which is fit to three peaks. The deconvoluted Ru spectrum shows two pairs of doublets with a spin-orbit splitting of 4.2 eV and a separation of ~1.2 eV, which suggests the presence of both metallic and oxidized Ru in the near-surface region.[45, 46] The metallic Ru 3d doublet is located at a binding energy of 280.8 eV and eV 285 eV, for the Ru $3d_{5/2}$ and Ru $3d_{3/2}$, respectively. The oxidized Ru 3d doublet is located at a binding energy of 282 eV and 286.2 eV. It is worth noting that there is considerable debate in the literature in relation to interpretation and fitting of the Ru 3d core-level.[47] Peaks in this location have also been assigned to satellite peaks, the RuO_2 plasmon and changes in Ru surface. [48, 49, 50] The presence of higher binding energy oxides has also been reported in nanoparticle systems,[45] however, detailed assessment of the oxide compositions is precluded to due to overlap with the C 1s peak. The O 1s shown in Fig. 2(b) is centered at a binding energy of 530 eV, typical of ITO.[51] The shoulder peak in the O 1s envelope is assigned to Ru oxides, typically observed ~532 eV and organic C–O/C=O bonds associated with the carbon, usually seen from 530-534 eV.[47]

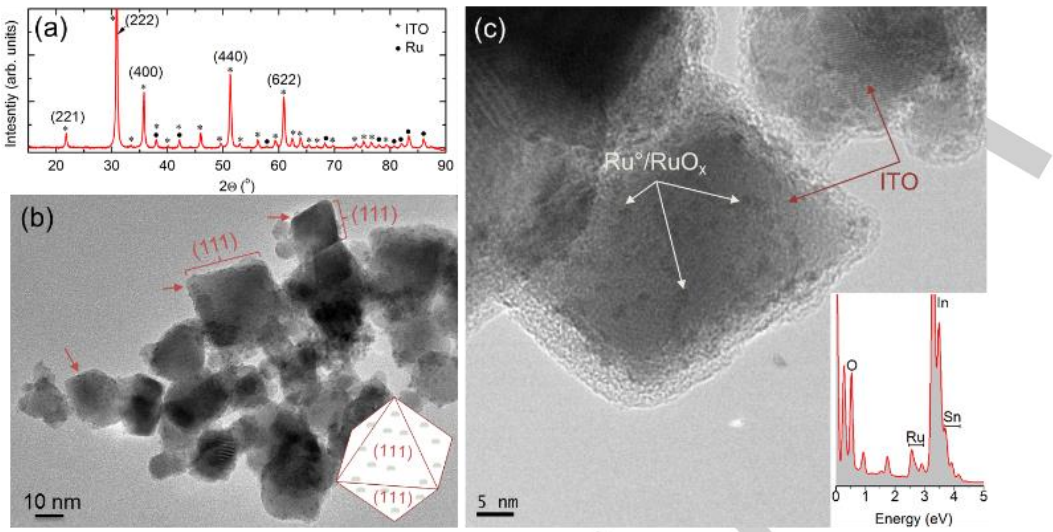

Figure 1. (a) X-ray powder diffraction pattern of the as prepared Ru/RuO_x/ITO powder. Peaks assignment according to the ICDD-JCPDS database for ITO (JCPDS 01-088-1734) and Ru° (JCPDS 01-088-0773). (b) TEM images of as prepared Ru/RuO_x/ITO composite. The red arrows point to some of the ITO nanocrystals, with cubic structure delineated typically by (111) planes (octahedral). (c) HRTEM image of Ru/RuO_x NP decoration of ITO nanocrystals and (inset) corresponding EDX spectrum.

The Ru concentration estimated by XPS using the Ru 3s as shown in the survey spectrum (Fig. 2 (c)) due to the Ru 3d overlap with the C 1s, was determined to be ~4 wt%, which is in excellent agreement with multiple-point, averaged EDX analysis (see Supporting Information, Table S1).

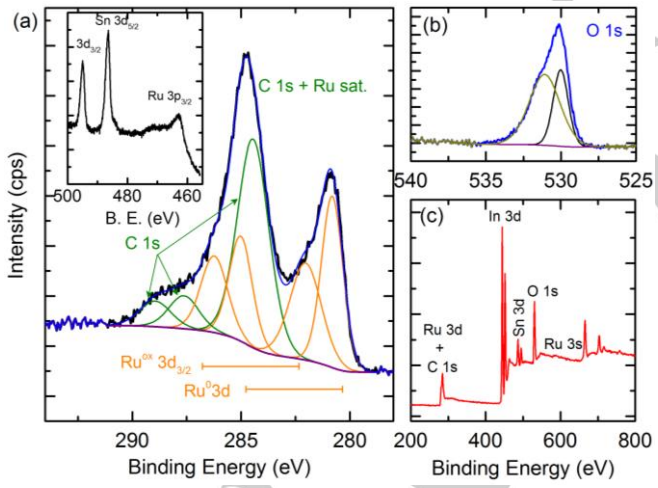

Figure 2. XPS spectra acquired from as-synthesized Ru/RuO_x nanoparticles immobilized on the surfaces of ITO nanocrystal powder of (a) Ru^{ox}, Ru° and C 1s core-level emission, (b) O 1s core level, and (c) survey spectrum of the Ru/RuO_x/ITO material.

Galvanostatic discharge-charge testing in Fig. 3(a) of carbon-based, ITO and Ru-functionalized ITO cathodes, and carbon-based cathodes in TEGDME and DMSO electrolyte-containing Li-O_2 batteries confirmed that Ru/RuO_x nanoparticle decoration of ITO significantly lowers the cell recharge potential with respect to ITO alone, and with respect to a typical carbon-based cathode. Despite differences in the BET-determined effective surface area (25.6 $m^2 g^{-1}$ for ITO and 80 $m^2 g^{-1}$ for carbon black), coatings of ITO on the gas diffusion layer current collector displayed almost the same charge and discharge potential plateaus of a carbon coated GDL cathode (Fig. 3a). As demonstrated by Zhou *et al.*, ITO is a stable conductive support showed no obvious catalytic activity toward either ORR and OER processes. During OER (charging), ITO maintains a similar overall overpotential to the carbon cathode.[28] In Fig. 3, the cathodes were cycled at the limited capacity of 1.0 mAh cm^{-2} with voltage limits of 2.25 and 4.40 V (*vs.* Li/Li^+) at a current density of 0.05 mA cm^{-2} and all the cathodes contained PVDF-HFP as the binder.

In both cases, ITO and Ru/RuO_x/ITO cathodes displayed similar discharge potentials of 2.7 V in TEGDME and 2.8 V in DMSO-based electrolytes. Although some authors have reported differences of 0.19 V between RuO_2 catalysed cathodes and non-catalysed cells (at least up to the initial 14% discharge capacity), such differences were negligible in our Li-O_2 cells discharged in the same electrolyte.[52] In this case, the main factor influencing the discharge potential in our cells is the electrolyte composition and consistent ORR behaviour as Li_2O_2 is formed within all cathodes, as has been observed with other oxygen cathodes based on Co_3O_4.[53] As such, Li_2O_2 formation as indicated by the potential is consistent to a defined DOD for carbon, ITO and Ru/RuO_x/ITO cathodes in the same electrolyte during discharge at this rate. On recharge, the presence of Ru/RuO_x lowers the charge overpotential in all cases. We observe the best overpotential reduction in DMSO-based systems, as shown in Fig. 3(b), where the charge overpotential is reduced to 3.25-3.50 V, and maintained below the decomposition potential for DMSO. When the binder is replaced with fluorine-free CMC (Fig. 3(c)), we observe that in DMSO electrolyte, Ru/RuO_x/ITO cathodes have a higher discharge potential and lower charge overpotential compared to those in TEGDME, and thus a significantly improved

overall energy efficiency during cycling. The behaviour of the GDL is important and actively contributes to the overall capacity in a way that is similar to some carbons. We reported previously[54] that GDL activity in Li-O_2 batteries is considerable and for the present work small areas of the accessible GDL surface does actively contribute to discharging and charging (see Supporting Information Fig. S2). GDL behaves somewhat similar to the ITO-only cathodes but with a reduced cycle life at 100% efficiency and a typical increase in overpotential during cycling. The coverage of this active GDL surface by ITO and Ru/RuO_x/ITO in significant quantities of binder, as will be shown, successively improves the overall cycling response and stability, even when toroidal Li_2O_2 forms on the GDL while Li_2O_2 of layered morphology forms on and within the ITO decorated with Ru/RuO_x.

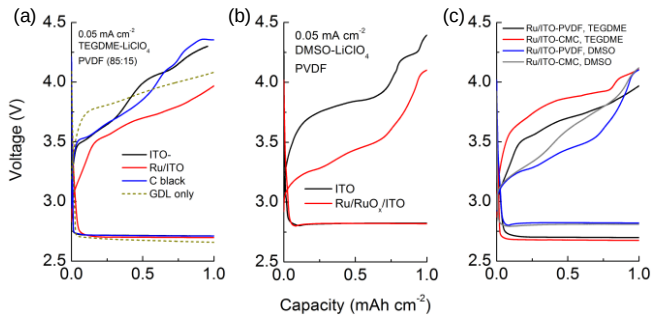

Figure 3. (a) Galvanostatic discharge and charge profiles acquired at 0.05 mA/cm^2 with 20 h of discharge, 20 h of charge, at a capacity-limit depth of discharge of 1 mAh/cm^2 for ITO, Ru/RuO_x/ITO and carbon black-coated GDL cathodes in TEGDME-$LiClO_4$ using PVDF binder. Profiles are show after the 5th cycle. (b) Galvanostatic discharge and charge profiles under similar conditions for Ru/RuO_x/ITO cathodes using PVDF or CMC binders. (c) comparison of discharge-charge profiles of Ru/RuO_x/ITO cathode in TEGDME and DMSO under similar conditions using CMC and PVDF binders.

Accordingly, the voltage gap between charge-discharge at 0.5 mAh cm^{-2} was reduced to just 0.62 V for Ru/RuO_x/ITO compared to 1.02 V for the ITO cathode in DMSO electrolyte (Fig. 3b), and 1.0 V for Ru/RuO_x/ITO compared to 1.3 V for ITO in TEGDME based electrolyte. A lower voltage gap of 0.88 V, at 1.25 mAh cm^{-2} for Ru/RuO_x/ITO cathodes, has been reported in a LiTFSA-triglyme based electrolyte.[28] In the same experimental condition, a voltage gap of 1.48 V for Super P carbon based cathodes was observed. The larger difference in overvoltage between non-catalysed and catalysed cathodes in glyme-based electrolytes is consistent with a higher content (7 wt. %) of Ru/RuO_x nanoparticles on the ITO support. The content of the Ru/RuO_x nanoparticles supported on ITO nanocrystals is ~4 wt. % in our case, and importantly, the 1-2 nm Ru/RuO_x particles are more uniformly distributed across the surface of the ITO at this wt%. Compared to Ru supported on reduced graphene oxide for example, 1-2 nm Ru/RuO_x NPs on ITO nanocrystals avoid graphene sheet encapsulation, which can reduce catalytic NP surface reactivity during OER, decreasing round trip efficiency and masking the effect on electrolyte stability.

Galvanostatic cycling tests at a 0.05 mA cm^{-2} rate with a limited capacity of 1.0 mAh cm^{-2} for the ITO cathodes in both TEGDME and DMSO electrolytes in Fig. 4(a,c), showed the ability of the ITO material to store the discharge products, and facilitate their decomposition during charging. In both cases, the two Li-O_2 cells behaved similarly in both electrolytes with coulombic efficiencies lower than 90% until the 5th cycle (Fig. 4 (a,b)). However, in DMSO, ITO nanocrystal-only cathodes allowed 19 efficient discharge-charge cycles (determined by fixed discharge time of 20 h), as shown in in Fig. 4(c,d) compared to 12 cycles observed in TEGDME electrolyte, suggesting that the DMSO reactivity supported the electrochemical removal of passivating reduction products during charging.[55]

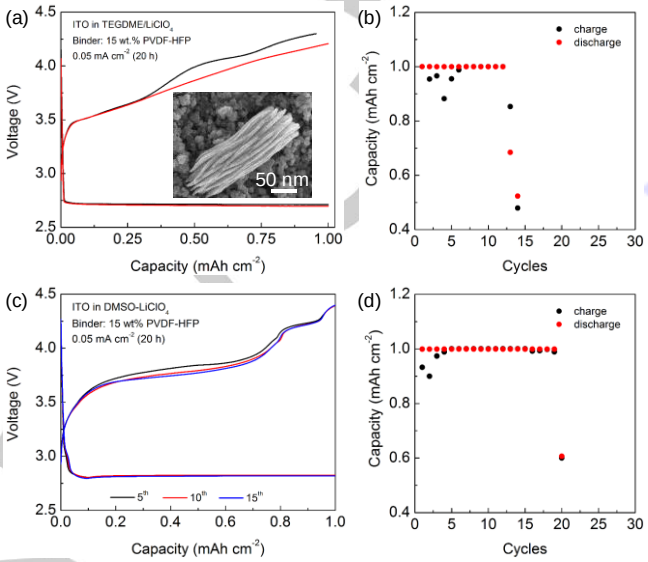

Figure 4. (a) Galvanostatic discharge and charge profiles, and (b) cycle life, acquired at 0.05 mA/cm^2 with 20 h of discharge, 20 h of charge, at a capacity-limit depth of discharge of 1 mAh/cm^2 for ITO cathodes in TEGDME-$LiClO_4$ and similarly (c,d) for DMSO-$LiClO_4$ using PVDF binder. Inset (a): SEM image of the layered Li_2O_2 discharge product formed on ITO during discharging.

FESEM analysis was used to identify the morphology of the discharge products on the different Ru/RuO_x/ITO and ITO cathodes at full depth of discharge (Fig. 4(a) inset). For the cathodes discharged in TEGDME, a low volumetric density of dispersed disc-shaped Li_2O_2 particles was obtained on the ITO surface. Such particles evolved to a dense cover of toroidal shaped Li_2O_2 in the Ru/RuO_x/ITO discharged cathodes. In DMSO (see Supporting Information, Fig. S3) with a high donor number (DN), we find an exceptional increase in the particle size on the Ru/RuO_x/ITO that is possibly from solution mediated Li_2O_2 growth and subsequent re-deposition onto the growing Li_2O_2. [56]

Better discharge product decomposition during charging became possible by pairing DMSO with Ru/RuO_x/ITO cathodes. Figures 5 (a, b) show the combined effect of the DMSO solvent and the OER catalytic action of Ru/RuO_x nanoparticles in reducing the charge overpotential of ITO-based cathodes, which allowed the Li-O_2 cell to deliver 32 stable and reversible discharge-charge cycles at 100% Coulombic efficiency. This corresponds to an additional 520 h of cycling operation for the Ru/RuO_x/ITO cell with respect to that of the ITO cathode in DMSO electrolyte (from a 4 wt% addition of Ru/RuO_x in 1-2 nm form), and better cycling compared to the Ru/RuO_x/ITO cathode-containing cells in TEGDME electrolyte (Fig. 5(c,d)). Furthermore, about 50% of the recharge process occurred at overpotentials <3.5 V.

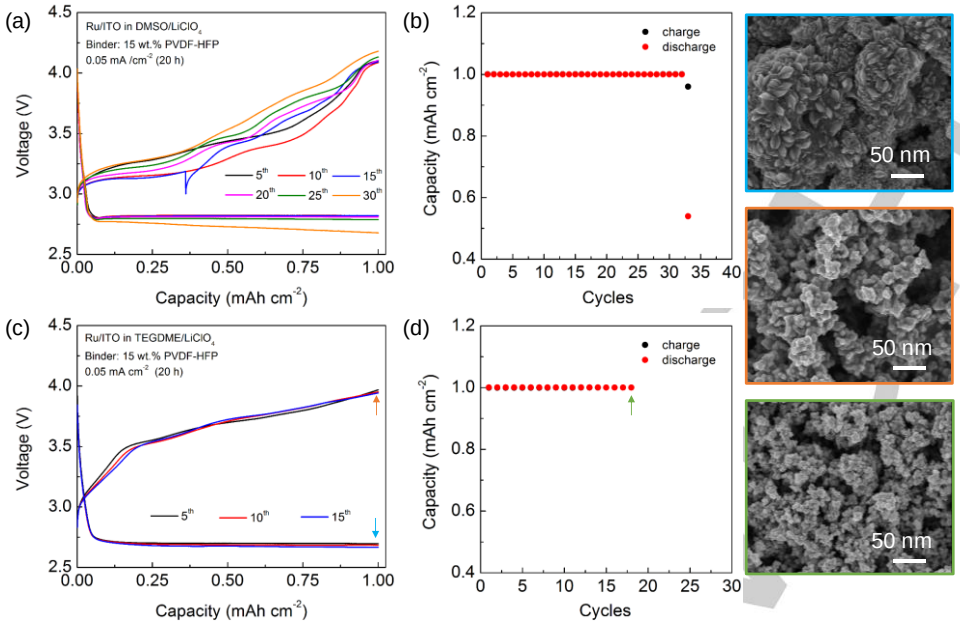

Figure 5. (a) Galvanostatic discharge and charge profiles, and (b) cycle life, acquired at 0.05 mA/cm^2 with 20 h of discharge, 20 h of charge, at a capacity-limit depth of discharge of 1 mAh/cm^2 for Ru/RuO$_x$/ITO cathodes in TEGDME-LiClO$_4$ and similarly (c,d) for DMSO-LiClO$_4$ using PVDF binder. SEM images of the Li_2O_2 discharge product formation and decomposition formed on Ru/RuO$_x$/ITO during discharging, recharging and cycling for each cell are color coded to the arrows in (c) and (d).

This improvement is attributable to the efficient OER catalytic activity of Ru/RuO$_x$ nanoparticles, an effect that is not observed with GDL-only, carbon or ITO-only cathodes. SEM analysis (Fig. 5) confirms efficient removal of the discharge product after charging, and the morphology of the charged cathode after all efficient cycles shows a similar charged-state cathode structure.

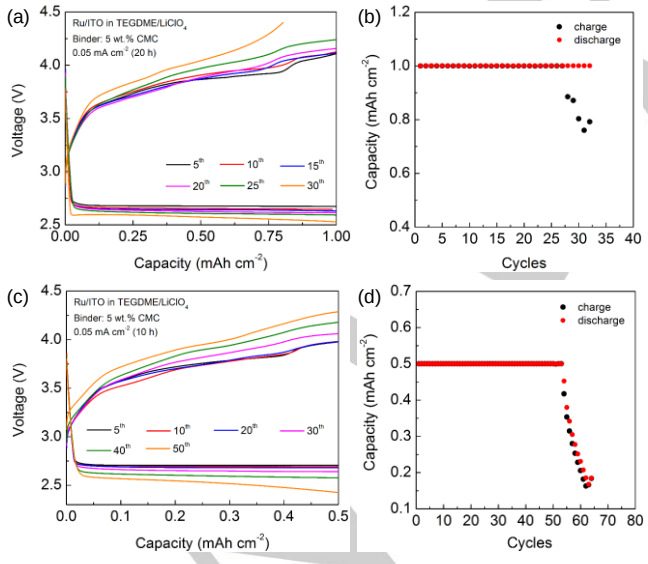

Figure 6. (a) Galvanostatic discharge and charge profiles, and (b) cycle life, acquired at 0.05 mA/cm^2 with 20 h of discharge, 20 h of charge, at a capacity-limit depth of discharge of 1 mAh/cm^2 for Ru/RuO$_x$/ITO cathodes in TEGDME-LiClO$_4$ and similarly (c,d) at a capacity-limit depth of discharge of 0.5 mAh/cm^2 using CMC binder.

A binder-dependent cycling performance of Super P carbon cathodes was previously observed in TEGDME/LITFSI electrolyte with capacities decreasing in the order PVDF > PTFE > polyethylene oxide (PEO) > poly vinylpyrrolidone (PVP).[44] This inspired the decision to replace the PVDF-HFP binder with CMC at the Ru/RuO$_x$/ITO cathode to determine the effect on cathode response. Traditionally, CMC is considered for Li-ion electrode manufacture as it allows processing in aqueous slurries rather than in environmentally unfriendly organic-compound-based slurries.[57] To date, very limited knowledge on the use of CMC for Li-O_2 cathodes is available from the literature. Zhang *et al.*[58] demonstrated that at low current densities (0.05 mA cm^{-2}), polymers with strong binding properties such as CMC decreased the discharge capacity of Ketjen black carbon cathodes in LiTFSI-tetraglyme electrolytes, compared to other binders that exhibited weaker binding properties when the polymer-to-carbon weight ratio was constant. This was in part because discharge product formation was sensitive to pore volume rather than surface area; blocking of smaller pores affects gas flow and mass transport.[59]

While Ru/RuO$_x$/ITO cathodes exhibit better energy efficiency in DMSO electrolyte, we also investigated the influence of Ru/RuO$_x$/ITO cathodes with CMC binders in TEGDME, to minimize side reactions involving fluorine that reduce TEGDME stability. Figure 6(a) shows the galvanostatic test of the CMC-bonded Ru/RuO$_x$/ITO cathode at 0.05 mA cm^{-2} with a limited capacity of 1.0 mAh cm^{-2}, in TEGDME electrolyte. The introduction of CMC into the cathode preparation does not improve (reduce) the charge overpotential but maintain cyclability without efficiency reduction (~30 cycles at 1.0 mAh cm^{-2} capacity limit, and almost 60 at 0.5 mAh cm^{-2}), whereas the GDL, carbon and ITO-only cathodes fades considerably in TEGDME. Figure S4 in the Supporting Information shows that the infilled discharge product is efficiently removed after the first recharge. The number

of discharge-charge cycles (Fig. 6(b)) is almost doubled compared to PVDF-HFP at the same 100% Coulombic efficiency (Fig. 5(d)), applied current density and capacity limit.

When we replaced the PVDF-HFP binder with CMC in the Ru/RuO_x/ITO cathode slurry and tested the cell with a DMSO electrolyte, the cell maintained very good cyclability as shown in Fig. 7. Discharging and recharging the cell at 0.05 mA cm^{-2} with a limited capacity of 0.5 mAh cm^{-2} leads to ~60 stable and reversible cycles at 100% Coulombic efficiency. The cell performance in DMSO with either binder is consistently good, and superior to controls using GDL and ITO only cathode formulations with either binder. In TEGDME, the recharge takes place at higher potential than in DMSO and the Li_2O_2 oxidation results in a higher parasitic electrochemical reaction rate.[60, 61] Under these conditions, the use of non-fluorinated binders may be effective and useful in prolonging the cycle life of the Li-O_2 cell in conjunction with cathodic formulations that reduce the Li_2O_2 decomposition overpotential efficiently. As the data shows, reduction in charge overpotential using OER catalysts and suitable electrolytes does not automatically improve cycle life, and overall cell stability and energy density is sensitive to catalytic activity and stability, electrolyte stability and the nature of the binder.

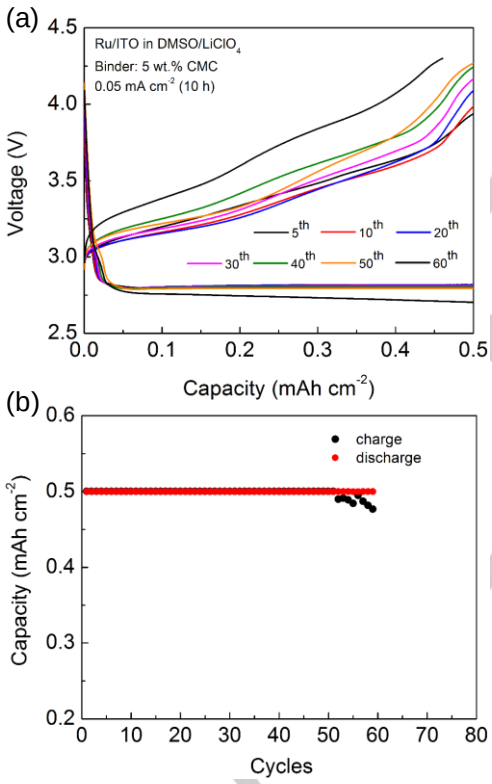

Figure 7. (a) Galvanostatic discharge and charge profiles and (b) cycle life, acquired at 0.05 mA/cm^2 with 10 h of discharge, 10 h of charge, at a capacity-limit depth of discharge of 0.5 mAh/cm^2 for Ru/RuO_x/ITO cathodes in DMSO-$LiClO_4$ using CMC binder.

The higher number of cycles observed in TEGDME electrolyte with CMC-bonded cathodes is not due to the greater relative quantity of Ru/RuO_x/ITO (95 wt % vs. 85 wt % in the CMC and PVDF-HFP slurries respectively) in the electrode. As shown in Supporting Information, Fig. S5, Li-O_2 cells with a TEGDME electrolyte tested to full depth of discharge and full recharge (between 2.15 V and 4.40 V, at 0.05 mA cm^{-2}) provide similarly high capacities of 8.3 mAh cm^{-2}. As a comparison, Zhou *et al.*[28] reported full discharge capacities of 2.5 mAh cm^{-2} at the very low applied current density of 0.025 mA cm^{-2} for a Ru/RuO_x/ITO cathode on Ni mesh in LiTFSA-(G3) electrolyte. By limiting the capacity to 1.8 mAh cm^{-2}, the discharge and charge curves of Ru/RuO_x/ITO showed capacity retention ranging from 80-100% over 50 cycles; the loading of Ru was 7 wt.%. In a separate study, they employed a higher Ru loading of 9.8 wt% supported on Sb-doped tin oxide[29] that demonstrated 50 cycles at full efficiency at 0.1 mA cm^{-2} with a capacity cut-off value of 750 mAh g^{-1}. Throughout, the effectiveness of the Ru/RuO_x at the defined DOD is always maintained compared to carbon and ITO-only cathodes with either binder in the cathode-friendly DMSO electrolyte. Cell death is usually found in our experiments due to Li degradation, before cathode failure.

Involving Ru/RuO_x surfaces on ITO or other supports is useful so that O_2 eventual evolution matches the O_2 consumed during discharge within as low an oxidation overpotential as possible, without enhancing Li*R*CO_3 species formation and parasitic chemistry that affects cell stability. Under similar conditions with PVDF or CMC binders, the formation of parasitic species that affect efficiency rechargeability, well known for DMSO and TEGDME with simpler carbon cathodes, are mitigated when the Ru/RuO_x NPs are present. ITO activity and stability during cycling has been assumed in recent reports. As previously reported,[22] Ru and Ru-oxides are promoters of OER rather than the ORR processes. In solution-based cross-coupling reactions and catalysis, we previously showed that catalyst nanoparticle leaching is prevalent in the catalytic processes involving other metals such as Pd and from enhanced interfacial activity in the presence of an oxide overlayer.[62] It may be possible that such effect contribute to the present work. In previous studies involving Ru./ITO for Li-O_2 systems, the stability of the Ru and the ITO was not examined. Here, we ensure a significant surface area is available to electrochemical reactions, even when a co-catalyst Ru metal is immobilised on these surfaces. To test the stability of ITO and Ru/RuO_x NPs, we investigated the cathode materials in various cells with both electrolytes and binder, in as-prepared conditions and also after discharging and charging. For Li_2O_2 oxidation mechanisms to be maintained by interfacial catalysis at Ru/RuO_x–Li_2O_2 interfaces they must remain active even when the ITO is deteriorated, cycle after cycle.

The nature of the Ru/RuO_x interface to ITO, and the stability of the ITO itself during discharge and charge were examined using high resolution XPS and XRD. XRD diffraction patterns (Fig. 8(a)) revealed Li_2O_2 as the only crystalline product deposited around the Ru/RuO_x/ITO cathode surface after full discharge in TEGDME. In DMSO however, crystalline LiOH and LiOH·H_2O were detected at full depth of discharge, confirming that DMSO undergoes decomposition with prolonged exposure to Li_2O_2[61], while Ru/RuO_x ensures continued cyclability and discharge product decomposition.

After full recharge in TEGDME, we note that Li_2O_2 is fully decomposed (within detection limits) in the presence of the Ru/RuO_x/ITO cathode with a PVDF binder (Fig. 8(b)). In Fig. 8(c) remnant Li_2O_2 is found after full recharge when a CMC binder is

used, together with Li_2CO_3 formed in the presence of carbon from the binder (but not from the GDL). In Fig. 8(b), XRD shows evidence that the ITO support of the Ru/RuO_x/ITO system is inherently unstable in the presence of PVDF binders - this does not affect the catalytic effect of the Ru/RuO_x based on cycling tests and microscopy. The crystalline Sn-doped In_2O_3 material is decomposed, while all other crystalline phases remain as expected from efficiency discharge and charge.

To identify the composition of phases in conjunction with XRD analysis, we conducted XPS on charged cathode formulations after initial discharge under identical electrochemical conditions to those in Fig. 8. Figure 9 shows the resulting survey spectra for Ru/RuO_x/ITO cathode materials in DMSO (with a PVDF binder in this case for comparison with Fig. 8) and in TEGDME with a CMC binder. Clear differences are noted in the intensity reduction of the In core-level photoemission spectra when a PVDF binder is used. XPS data together with XRD clarifies the instability of the cathode supporting materials. However, the effectiveness of Ru/RuO_x is maintained, even when the In_2O_3 component is decomposed allowing Ru/RuO_x particles to redistribute over the discharge product formed within the ITO support nanomaterial.

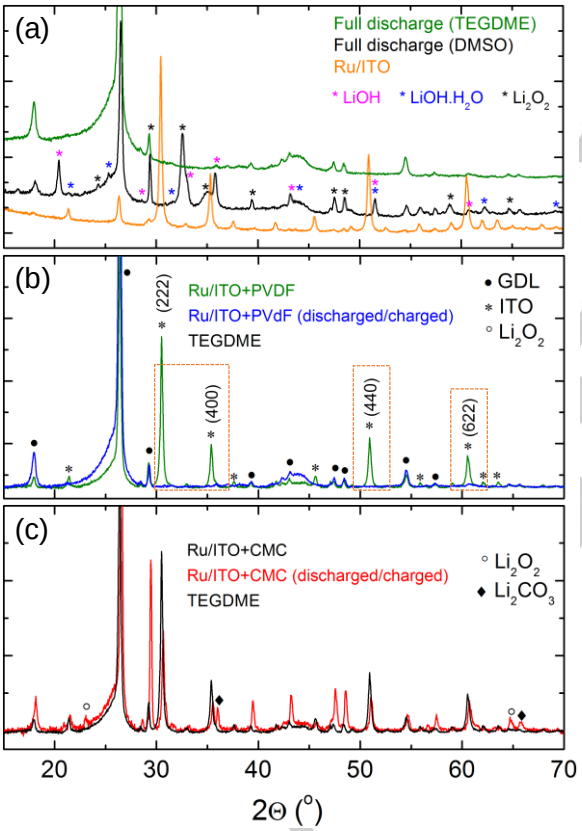

Figure 8. (a) XRD patterns from pristine Ru/RuO_x nanoparticle-decorated ITO nanocrystalline powder and after full discharge in DMSO and TEGDME-based electrolytes with PVDF binder. (b) Ru/RuO_x/ITO mixed with PVDF and after full discharge and recharge. (c) XRD patters for Ru/RuO_x/ITO mixed with CMC, and after discharge and full recharge.

The crystalline nature of ITO is amorphized and partially decomposed in TEGDME with F-containing binders (Fig. 8(b)). In DMSO, the ITO is entirely decomposed leaving residual atomic In detectable within the cathode and a significant F peak (Fig. 9), but significantly, the Sn dopant of ITO remains in a similar relative quantity to as-received $Sn:In_2O_3$ (ITO). The use of a CMC or carbon-based binder helps to avoid ITO nanocrystal deterioration. Ru/RuO_x remains in all cases throughout cycling and while it has an oxide overlayer, its core Ru metallic nature remains intact in all binder and electrolyte combinations as confirmed by photoelectron emission measurements in Fig. 9. Some oxidation of Ru^0 is found after the first cycle in TEGDME with CMC. The relative concentration notably remains similar to the starting amounts. The cyclability is limited in the presence of PVDF, even when Ru/RuO_x catalysts lower the charge overpotential to efficiently decompose the Li_2O_2 discharge product regardless of the deterioration of the non-carbonaceous host material.

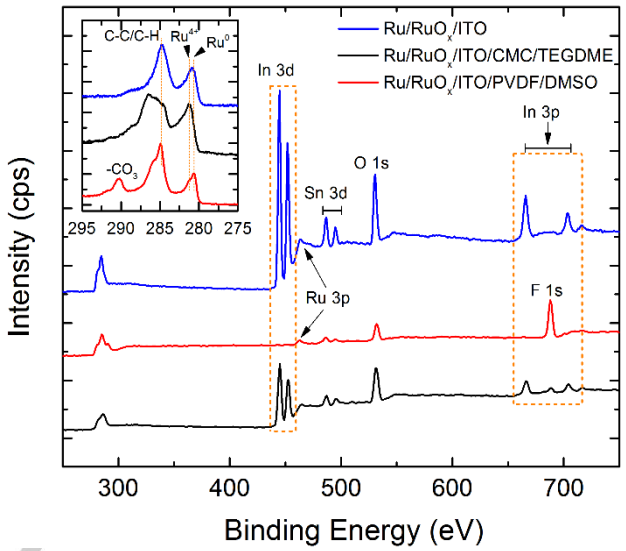

Figure 9. (a) XPS spectra from pristine Ru/RuO_x nanoparticle-decorated ITO nanocrystalline powder and after full cycle (discharge and recharge) in DMSO-PVDF and TEGDME-CMC electrolyte-binder systems.

The cause is due to the decomposition or modification to the ITO nanocrystal support, which is shown here be unstable in the presence of PVDF when the binder undergoes dehydrofluorination. Recent studies highlighted the instability of PVDF-HFP binder towards Li_2O_2. The PVDF backbone can be subjected to dehydrofluorination in the Li-O_2 environment. The release of fluoride ions is responsible of the formation of LiF [63] and also HF. This reaction occurs with LiO_2 superoxide anions and can contribute to the *in-situ* formation of H_2O, LiOH, Li_2O_2 and H_2O_2, a mechanism outlined in detailed elsewhere.[43, 64] We postulate that the liberated F atoms and the generation of HF in the presence of H_2O and H_2O_2 leads to wet chemical etching of the ITO support leaving the Ru species present and active as OER catalysts - this chemistry is pronounced in DMSO and PVDF. The standard wet chemical etchant for ITO is $HF:H_2O_2:H_2O$ (1:1:10 v/v) to give an etch rate of 125 Å s^{-1}. The ITO deterioration process occurs during the very first recharge, yet does not negatively affect the overall discharge process, and recharge processes during successive cycling.

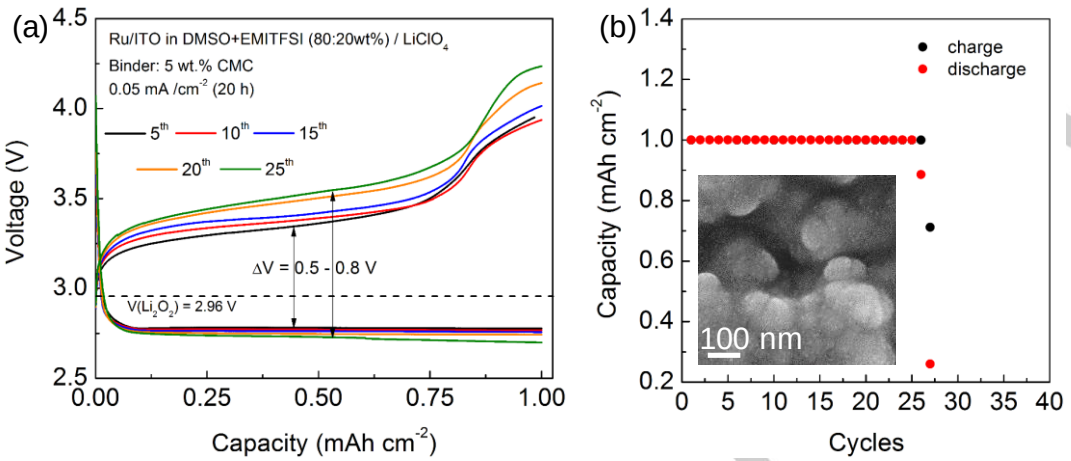

Figure 10. (a) Galvanostatic discharge and charge profiles and (b) cycle life, acquired at 0.05 mA/cm^2 with 20 h of discharge, 20 h of charge, at a capacity-limit depth of discharge of 1 mAh/cm^2 for Ru/RuO_x/ITO cathodes in a mixed DMSO (80 wt%)-EMITFSI (20 wt%)-$LiClO_4$ electrolyte using CMC binder. The inset SEM image in (b) shows the morphology of the discharge product.

A separate investigation did prove that a stable, thin SEI forms on carbon based Li-O_2 cathode that were Ru-catalyzed in DMSO[46], and when the same cathode was replaced in a cell with a fresh Li anode, efficient cycling continued.

Lastly, the Ru/RuO_x/ITO nanocrystal cathodes contribute to the improvement of overall cycling efficiency in DMSO and TEGDME electrolytes by improving OER compared to the carbon-based material, because the Ru/RuO_x remains active. We used this cathode formulation with F-free CMC with a higher ionic conductivity DMSO-EMITFSI ionic liquid mixture electrolyte, where Li_2O_2 forms via different processes compared to aprotic electrolyte systems of single solvents such as glymes, ethers and sulfoxides alone. Figure 10 shows that over 25 cycles at 100% Coulombic efficiency, the voltage gap was maintained between low values of 0.5 – 0.8 V, significantly boosting the cell efficiency by maintaining a voltage gap <1 V, which is similarly achieved by redox mediator electrolytes.[38] Zhao et al. in separate investigations on ORR and OER processes, have also shown enhanced performance in aprotic mixtures of DMSO and other ionic liquids, whose cations were stable against superoxide reactions.[65, 66] SEM analysis (Fig. 10(b) inset) shows that the Li_2O_2 phase forms as a high density of nanoparticle-like structures on and within the Ru/RuO_x/ITO cathode structure, and each discharge retains a very consistent potential while OER recharge processes retain a low overpotential.

Conclusions

An ITO nanocrystal cathode material with 1-2 nm RuO_x/Ru nanoparticles immobilized across its surface was examined as a cathode component for Li-O_2 batteries. We examined the difference between the structural stability of the RuO_x/Ru/ITO material with F-containing and carbon based binders in DMSO and TEGDME electrolytes, and examined the effectiveness of OER catalysis from the RuO_x/Ru in the case where structural degradation of the ITO support material occurs or not. When formulated as a carbon-free cathode slurry, the cathode demonstrates efficient OER processes, significantly reducing the recharge overpotential, and maintaining a consistent cycling discharge potential. The use of CMC binders avoids PVDF-based side reactions with TEGDME and DMSO, thus improving efficiency cyclability while maintaining OER catalyst activity of Ru/RuO_x NPs towards Li_2O_2 decomposition.

The findings demonstrate that binders such as CMC in Ru/RuO_x/ITO cathode slurries avoid F-based side reactions and improve cycle life. Overpotential reduction does improve overall energy density, but cathode, electrolyte, binder and catalyst stability are critical for long term cycling. The deterioration of the ITO nanocrystal cathode support material in the presence of F-species from HF etching of In_2O_3 is proven. Redistribution of Ru/RuO_x NPs ensures beneficial catalytic activity in DMSO and PVDF, mitigating severe deterioration of discharge and charge potentials, capacity, and cathode cycle life. The use of a CMC or carbon-based binder avoids ITO nanocrystal deterioration (Ru remains in both cases throughout cycling). In mixed DMSO-EMITFSI ionic liquid electrolytes, Li-O_2 cells cycle very well and maintain a very low charge overpotential such that the voltage gap between discharge and charge is kept between 0.5 – 0.8 V.

The investigation confirms the sensitive dependence of cycling performance and capacity health on the synergy between all cell components, but importantly shows that cycling is aided in carbon-free cathodes by the use of stable OER catalysts. Li_2O_2 is consistently decomposed, implying a redistribution of Ru/RuO_x species during ITO cathode rearrangement during charging, and the catalytic benefit appears to be maintained during successive cycling. Solution-processable CMC binders offer significant cycle life benefits in conjunction with catalysts that improve energy efficiency even at the expense of marginally higher charge overpotentials. Modified electrolytes including those with redox mediators may prove useful in extending cycle life, but OER catalyst NPs can remain effective in reactive electrolyte where support material dissolution occurs, or where redistribution of catalysts onto discharge products retains their effectiveness.

Experimental Section

Synthesis of the Ru/RuO_x/ITO electro-catalyst

In a typical preparation, 100 ml of ethylene glycol was mixed with 410 mg of nanocrystalline powdered ITO (Sigma Aldrich) followed by adding of 95 mg $RuCl_3.6H_2O$ to form a suspension with pH = 13.39. After stirring for 1h, 5ml of 0.5M NaOH was added and the suspension was refluxed for 3 h under inert atmosphere (Ar). After cooling down to room temperature, formic acid was added to the reaction mixture until the pH was ~3.6. Subsequently, the suspension was stirred overnight at ambient conditions. As prepared Ru/RuO_x/ITO particles were filtered and dried under vacuum at 90°C overnight. All the chemicals used in the material preparation were purchased from Sigma Aldrich.

Structural and morphological characterization

The X-ray diffraction analysis was carried out using a high resolution Philips X'pert MPD powder diffractometer, equipped with Cu Kα radiation (V = 40 kV, I = 30 mA) and a curved graphite secondary monochromator. The diffraction profiles were collected in the 2θ range between 15° and 90°, with an acquisition step of 0.018° and a time per step of 10 s using a solid state PIXcel-1D detector with 255 active channels. The sample morphologies were examined using a scanning electron microscope (SEM) FEI Quanta Inspect 200LV. Nitrogen adsorption isotherms at 77 K were recorded with an ASAP 2010 C Instrument (Micromeritics). The specific surface area of the samples was calculated by BET method within the relative pressure range of 0.05 to 0.2. X-ray Photoelectron Spectroscopy (XPS) was acquired using a KRATOS AXIS 165 monochromatized X-ray photoelectron spectrometer equipped with an Al Kα (hv = 1486.6 eV) X-ray source. The collection take-off angle was 90° and all spectra were reference to the C 1s peak at 284.8 eV. Peaks were fit a Shirley background and Gaussian-Lorentzian line shape.

Transmission Electron Microscopy (TEM) and energy dispersive X-ray (EDX) spectroscopy was carried out using a JEM2010-TEM operating at 200 kV equipped with an Oxford X-Max 80 detector and Inca analysis software.

Li-O_2 cell assembly and electrochemical characterization

The O_2 electrode was prepared as a thin film over carbon paper gas-diffusion layer (SIGRACET GDL-24BC, SGL Technologies). An N-methyl-2-pyrrolidone (NMP) slurry of Ru/RuO_x/ITO with poly(vinylidene fluoride co-hexafluoropropylene) PVDF-HFP (Solvay, Kynar) as binder in a weight ratio of 85:15 was deposited over GDL using a doctor blade technique. The same cathode slurries were prepared with a Sodium carboxymethyl cellulose CMC (Aldrich) binder. In that case, a weight ratio of 95:5 was considered. The films were then dried at 55 °C overnight to obtain a composite cathode of about 0.9 ± 0.1 mg cm^{-2} of Ru/RuO_x/ITO material. A cathode with only ITO (Aldrich) and PVDF-HFP (weight ratio of 85:15) was also prepared for comparison. The cathodes were dried in the vacuum at 120°C for 6 h. The cathodes were pre-cut with an EL-Cut puncher type (EL-Cell, GmbH) to obtain discs of bare GDL of 2.54 cm^2 geometrical area with an average weight of 25.7 ± 0.2 mg. All data reported here accounts for the well-known activity of the carbon-based GDL current collector (only its accessible surface), and active mass/binder mixtures do not uniformly coat all GDL surfaces. GDL actively participates in the response without effects from binder-electrolyte interactions, but has a limited cycle life. The specific electrochemical responses shown for various binder, ITO, Ru/RuO_x materials in DMSO and TEGDME were compared to GDL-only controls. All capacities calculated include all active materials, i.e. the cathode mass values were typically: Ru-ITO-PVDF-GDL = 27 mg; Ru-ITO-CMC-GDL = 28 mg; ITO/PVDF/GDL = 27 mg.

A lithium disc (18 × 0.2 mm, Chemetall s.r.l.) was used as anode and glass fibre (18.0 × 0.65 mm, ECC1-01-0012-A/L) saturated with the electrolyte was used as the separator. Solutions of 0.5 M $LiClO_4$ (Aldrich) in tetra (ethylene glycol) dimethyl ether (tetraglyme, Fluka) and 0.5 M $LiClO_4$ (Aldrich) in dimethyl sulfoxide (DMSO, Aldrich) were used as the electrolytes. Prior to use, the electrolyte was treated with molecular sieves (4.0 Å beads, 8-12 mesh, Aldrich) inside a glove box. The Li-O_2 cell was then assembled in an Ar-filled dry glove box (MBraun Labstar) using an ECC-Air electrochemical cell (EL-Cell, GmbH) configuration with openings allowing oxygen to enter and exit through the cathodic side. The cells were galvanostatically discharged by an Arbin BT-2000 battery tester at room temperature from the open circuit voltage (OCV) to 2.25 V vs. Li^+/Li at a discharge current density of 0.05 mA cm^{-2} after 6 h of rest at OCV. Charge/discharge tests were also carried out in controlled potential/time mode between 2.25 V and 4.30 V vs. Li^+/Li limiting the capacity to 1.0 mAh cm^{-2} (20 h of discharge and 20 h of recharge at the current density of 0.05 mA cm^{-2}) or at 0.5 mAh cm^{-2} (10 h of discharge and 10 h of recharge at the current density of 0.05 mA cm^{-2}). During discharge and charge, the Li-O_2 cells were continuously fed with pure dry oxygen (3.5 ml min^{-1}). Unless otherwise stated, all the voltages are referenced to Li^+/Li.

Acknowledgements

This research has received funding from the Seventh Framework Programme FP7/2007-2013 (Project STABLE) under grant agreement no. 314508. This work was also supported by Science Foundation Ireland (SFI) through an SFI Technology Innovation and Development Award under contract no. 13/TIDA/E2761. Support from the Irish Research Council New Foundations Award is gratefully acknowledged. G. C. acknowledges funding from a National University of Ireland Fellowship in the Sciences. This publication has also emanated from research supported in part by a research grant from SFI under Grant Number 14/IA/2581.

Keywords: Li-air battery • Li-O_2 battery • nanoparticle • energy storage • OER catalyst • electrolyte • cathode • nanocrystal • electrochemistry

[1] P. G. Bruce, S. A. Freunberger, L. J. Hardwick, J. M. Tarascon, *Nat. Mater.* **2011**, *11*, 19-29.
[2] Z.-W. Chang, J.-J. Xu, Q.-C. Liu, L. Li, X.-B. Zhang, *Adv. Energy Mater.* **2015**, *5*, 1500633.
[3] Y. Li, Z. Huang, K. Huang, D. Carnahan, Y. Xing, *Energy Environ. Sci.* **2013**, *6*, 3339–3345.
[4] R. Cao, J.-S. Lee, M. Liu, J. Cho, *Adv. Energy Mater.* **2012**, *2*, 816–829.
[5] J.-S. Lee, S. T. Kim, R. Cao, N.-S. Choi, M. Liu, K. T. Lee, J. Cho, *Adv. Energy Mater.* **2011**, *1*, 34–50.
[6] K. G. Gallagher, S. Goebel, T. Greszler, M. Mathias, W. Oelerich, D. Eroglu, V. Srinivasan, *Energy Environ Sci.* **2014**, *7*, 1555-1563.
[7] J.-J. Xu, Z.-L. Wang, D. Xu, L.-L. Zhang, X.-B. Zhang, *Nat. Commun.* **2013**, *4*.
[8] Y. Li, X. Wang, S. Dong, X. Chen, G. Cui, *Adv. Energy Mater.* **2016**, 10.1002/aenm.201600751.
[9] F. Marchini, S. Herrera, W. Torres, A. Y. Tesio, F. J. Williams, E. J. Calvo, *Langmuir* **2015**, *31*, 9236-9245.
[10] B. D. McCloskey, R. Scheffler, A. Speidel, D. S. Bethune, R. M. Shelby, A. C. Luntz, *J. Am. Chem. Soc.* **2011**, *133*, 18038-18041.
[11] Y. Shao, S. Zhang, C. Wang, Z. Nie, J. Liu, Y. Wang, Y. Lin, *J. Power Sources* **2010**, *195*, 4600-4605.
[12] J. Xiao, D. Mei, X. Li, W. Xu, D. Wang, G. L. Graff, W. D. Bennett, Z. Nie, L. V. Saraf, I. A. Aksay, J. Liu, J.-G. Zhang, *Nano Lett.* **2011**, *11*, 5071-5078.
[13] E. Yoo, T. Okata, T. Akita, M. Kohyama, J. Nakamura, I. Honma, *Nano Lett.* **2009**, *9*, 2255-2259.

[14] Y.-C. Lu, Z. Xu, H. A. Gasteiger, S. Chen, K. Hamad-Schifferli, Y. Shao-Horn, *J. Am. Chem. Soc.* **2010**, *132*, 12170-12171.
[15] H. Cheng, K. Scott, *J. Power Sources* **2010**, *195*, 1370-1374.
[16] A. Debart, J. Bao, G. Armstrong, P. G. Bruce, *ECS Trans.* **2007**, *3*, 225-232.
[17] A. Débart, A. J. Paterson, J. Bao, P. G. Bruce, *Angew. Chem. Int. Ed.* **2008**, *120*, 4597-4600.
[18] Q.-C. Liu, J.-J. Xu, D. Xu, X.-B. Zhang, *Nat. Commun.* **2015**, *6*.
[19] M. D. Bhatt, H. Geaney, M. Nolan, C. O'Dwyer, *Phys. Chem. Chem. Phys.* **2014**, *16*, 12093-12130.
[20] J. R. Harding, Y.-C. Lu, Y. Tsukada, Y. Shao-Horn, *Phys. Chem. Chem. Phys.* **2012**, *14*, 10540-10546.
[21] B. Sun, P. Munroe, G. Wang, *Sci. Rep.* **2013**, *3*, 2247
[22] H.-G. Jung, Y. S. Jeong, J.-B. Park, Y.-K. Sun, B. Scrosati, Y. J. Lee, *ACS Nano* **2013**, *7*, 3532-3539.
[23] J.-J. Xu, D. Xu, Z.-L. Wang, H.-G. Wang, L.-L. Zhang, X.-B. Zhang, *Angew. Chem. Int. Ed.* **2013**, *52*, 3887-3890.
[24] M. M. Ottakam Thotiyl, S. A. Freunberger, Z. Peng, P. G. Bruce, *J. Am. Chem. Soc.* **2013**, *135*, 494-500.
[25] B. D. McCloskey, A. Speidel, R. Scheffler, D. C. Miller, V. Viswanathan, J. S. Hummelshøj, J. K. Nørskov, A. C. Luntz, *J. Phys. Chem. Lett.* **2012**, *3*, 997-1001.
[26] Z. Peng, S. A. Freunberger, Y. Chen, P. G. Bruce, *Science* **2012**, *337*, 563-566.
[27] M. M. O. Thotiyl, S. A. Freunberger, Z. Peng, Y. Chen, Z. Liu, P. G. Bruce, *Nat. Mater.* **2013**.
[28] F. Li, D.-M. Tang, Y. Chen, D. Golberg, H. Kitaura, T. Zhang, A. Yamada, H. Zhou, *Nano Lett.* **2013**.
[29] F. Li, D. M. Tang, Z. Jian, D. Liu, D. Golberg, A. Yamada, H. Zhou, *Adv. Mater.* **2014**, *26*, 4659-4664.
[30] A. Riaz, K.-N. Jung, W. Chang, K.-H. Shin, J.-W. Lee, *ACS Appl. Mater. Interfaces* **2014**, *6*, 17815-17822.
[31] J.-B. Park, I. Belharouak, Y. J. Lee, Y.-K. Sun, *J. Power Sources* **2015**, *295*, 299-304.
[32] J. Xie, X. Yao, I. P. Madden, D.-E. Jiang, L.-Y. Chou, C.-K. Tsung, D. Wang, *J. Am. Chem. Soc.* **2014**, *136*, 8903-8906.
[33] Y. Chang, S. Dong, Y. Ju, D. Xiao, X. Zhou, L. Zhang, X. Chen, C. Shang, L. Gu, Z. Peng, *Adv. Sci.* **2015**, *2*.
[34] S. H. Oh, R. Black, E. Pomerantseva, J.-H. Lee, L. F. Nazar, *Nat. Chem.* **2012**, *4*, 1004-1010.
[35] D. Sharon, V. Etacheri, A. Garsuch, M. Afri, A. A. Frimer, D. Aurbach, *J. Phys. Chem. Lett.* **2012**, 127-131.
[36] D. Xu, Z.-l. Wang, J.-j. Xu, L.-l. Zhang, X.-b. Zhang, *Chem. Commun.* **2012**, *48*, 6948-6950.
[37] M. A. Schroeder, N. Kumar, A. J. Pearse, C. Liu, S. B. Lee, G. W. Rubloff, K. Leung, M. Noked, *ACS Appl. Mater. Interfaces* **2015**, *7*, 11402-11411.
[38] W.-J. Kwak, D. Hirshberg, D. Sharon, M. Afri, A. A. Frimer, H.-G. Jung, D. Aurbach, Y.-K. Sun, *Energy Environ. Sci.* **2016**.
[39] T. Liu, M. Leskes, W. Yu, A. J. Moore, L. Zhou, P. M. Bayley, G. Kim, C. P. Grey, *Science* **2015**, *350*, 530-533.
[40] J. Lu, Y. Jung Lee, X. Luo, K. Chun Lau, M. Asadi, H.-H. Wang, S. Brombosz, J. Wen, D. Zhai, Z. Chen, D. J. Miller, Y. Sub Jeong, J.-B. Park, Z. Zak Fang, B. Kumar, A. Salehi-Khojin, Y.-K. Sun, L. A. Curtiss, K. Amine, *Nature* **2016**, 377–382.
[41] E. M. Erickson, E. Markevich, G. Salitra, D. Sharon, D. Hirshberg, E. de la Llave, I. Shterenberg, A. Rozenman, A. Frimer, D. Aurbach, *J. Electrochem. Soc.* **2015**, *162*, A2424-A2438.
[42] N. Mozhzhukhina, L. P. Méndez De Leo, E. J. Calvo, *J. Phys. Chem. C* **2013**, *117*, 18375-18380.
[43] R. Black, S. H. Oh, J.-H. Lee, T. Yim, B. Adams, L. F. Nazar, *J. Am. Chem. Soc.* **2012**, *134*, 2902-2905.
[44] H. Geaney, C. O'Dwyer, *J. Electrochem. Soc.* **2016**, *163*, A43-A49.
[45] E. A. Paoli, F. Masini, R. Frydendal, D. Deiana, C. Schlaup, M. Malizia, T. W. Hansen, S. Horch, I. E. Stephens, I. Chorkendorff, *Chem. Sci.* **2015**, *6*, 190-196.
[46] M. A. Schroeder, A. J. Pearse, A. C. Kozen, X. Chen, K. Gregorczyk, X. Han, A. Cao, L. Hu, S. B. Lee, G. W. Rubloff, M. Noked, *Chem. Mater.* **2015**, *27*, 5305-5313.
[47] D. J. Morgan, *Surf. Interface Anal.* **2015**, *47*, 1072-1079.
[48] K. Reuter, M. Scheffler, *Surf. Sci.* **2001**, *490*, 20-28.
[49] H. Over, A. Seitsonen, E. Lundgren, M. Smedh, J. N. Andersen, *Surf. Sci.* **2002**, *504*, L196-L200.
[50] D. J. Morgan, *Surf. Interface Anal.* **2015**, *47*, 1072-1079.
[51] S. So, W. Choi, C. Cheng, L. Leung, C. Kwong, *Appl. Phys. A* **1999**, *68*, 447-450.
[52] E. Yilmaz, C. Yogi, K. Yamanaka, T. Ohta, H. R. Byon, *Nano Lett.* **2013**, *13*, 4679-4684.
[53] J. Zeng, C. Francia, J. Amici, S. Bodoardo, N. Penazzi, *RSC Adv.* **2015**, *5*, 83056-83064.
[54] H. Geaney, J. O'Connell, J. D. Holmes, C. O'Dwyer, *J. Electrochem. Soc.* **2014**, *161*, A1964-A1968.
[55] M. J. Trahan, S. Mukerjee, E. J. Plichta, M. A. Hendrickson, K. Abraham, *J. Electrochem. Soc.* **2013**, *160*, A259-A267.
[56] N. B. Aetukuri, B. D. McCloskey, J. M. García, L. E. Krupp, V. Viswanathan, A. C. Luntz, *Nat. Chem.* **2015**, *7*, 50-56.
[57] S. Lux, F. Schappacher, A. Balducci, S. Passerini, M. Winter, *J. Electrochem. Soc.* **2010**, *157*, A320-A325.
[58] E. Nasybulin, W. Xu, M. H. Engelhard, Z. Nie, X. S. Li, J.-G. Zhang, *J. Power Sources* **2013**, *243*, 899-907.
[59] S. R. Younesi, S. Urbonaite, F. Biorefors, K. Edstrom, *J. Power Sources* **2011**, *196*, 9835-9838.
[60] B. D. McCloskey, A. Valery, A. C. Luntz, S. R. Gowda, G. M. Wallraff, J. M. Garcia, T. Mori, L. E. Krupp, *J. Phys. Chem. Lett.* **2013**, 2989-2993.
[61] D. G. Kwabi, T. P. Batcho, C. V. Amanchukwu, N. Ortiz-Vitoriano, P. Hammond, C. V. Thompson, Y. Shao-Horn, *J. Phys. Chem. Lett.* **2014**, 2850-2856.
[62] G. Collins, M. Schmidt, C. O'Dwyer, J. D. Holmes, G. P. McGlacken, *Angew. Chem. Int. Ed.* **2014**, *53*, 4142-4145.
[63] C. V. Amanchukwu, J. R. Harding, Y. Shao-Horn, P. T. Hammond, *Chem. Mater.* **2014**, *27*, 550–561.
[64] H. Geaney, C. O'Dwyer, *Phys. Chem. Chem. Phys.* **2015**, *17*, 6748 - 6759.
[65] A. Khan, C. Zhao, *ACS Sus. Chem. Eng.* **2016**, *4*, 506-513.
[66] A. Khan, C. Zhao, *Electrochem. Commun.* **2014**, *49*, 1-4.

10.1002/cssc.201601301

WILEY-VCH

Entry for the Table of Contents

FULL PAPER

ITO nanocrystals with supported 1-2 nm Ru/RuOx NPs demonstrates efficient OER processes. The Ru/RuOx NPs have the greatest effect in DMSO electrolytes with a solution-processable F-free CMC binder. ITO is unstable from the first cycle and completely dissolves by chemical etching. Ru/RuOx NPs are redistributed and remain effective OER catalysts for Li_2O_2 during cycling. CMC binder avoids PVDF-based side reactions in both DMSO and TEGDME electrolytes, improving efficient cyclability.

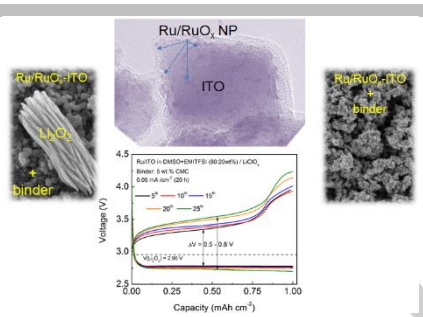

*Svetoslava Vankova, Carlotta Francia, Julia Amici, Juqin Zeng, Silvia Bodoardo, Nerino Penazzi, Gillian Collins, Hugh Geaney, and Colm O'Dwyer**

Page No. – Page No.

The Influence of Binders and Solvents on the Stability of Ru/RuO$_x$ OER Catalyst Nanoparticles on ITO Nanocrystals in Cycled Li-O$_2$ Battery Cathodes